ISSN 1070-3284, Russian Journal of Coordination Chemistry, 2018, Vol. 44, No. 1, pp. 21–31. © Pleiades Publishing, Ltd., 2018.

Crystal Structures and Biological Studies Two Novel Zinc Complexes Derived from *para*-Vanillin and Acetylacetone. Two New Precursors for Preparation ZnO Nanoparticles[1]

M. Jafari[a], M. Salehi[a, *], M. Kubicki[b], and A. Khaleghian[c]

[a] *Department of Chemistry, College of Science, Semnan University, Semnan, Iran*
[b] *Faculty of Chemistry, Adam Mickiewicz University, Umultowska 89b, 61-614 Poznan, Poland*
[c] *Biochemistry Department, Faculty of Medicine, Semnan University of Medical Sciences, Semnan, Iran*
**e-mail: msalehi@semnan.ac.ir*

Received May 4, 2017

Abstract—In the present study, two new zinc complexes with the chemical formulas of [Zn(2-Ampy)(Acac)$_2$] (**I**) and [Zn(*p*-Van)$_2$(H$_2$O)$_2$] (**II**) were synthesized and characterized by FT-IR, ^{1}H NMR, and UV-Vis spectroscopy. Moreover, the crystal structures of the complexes were determined by X-ray diffraction technique. Single-crystal X-ray diffraction analyses (CIF files CCDC nos. 1513672 (**I**) and 1513673 (**II**)) revealed that complex **I** has a distorted square pyramid environment, and complex **II** has a distorted octahedral geometry. The complexes were also screened for in vitro antibacterial activities against some bacteria. The results show that complexes have the effective antibacterial activities. The complexes were employed to prepare ZnO nanoparticles by the combustion synthesis method at 700°C for 8 h. The nanoparticles were characterized, using powder X-ray diffraction analysis (PXRD), scanning electron microscopy and transmission electron microscope. PXRD analysis showed the presence of pure phase in both samples. Furthermore, the crystallite size was approximately 37 and 42 nm for ZnO prepared from complexes **I** and **II**, respectively.

Keyword: biological studies, X-ray diffraction analysis, ZnO, nanoparticles, zinc complexes

DOI: 10.1134/S1070328418010086

INTRODUCTION

In recent years, metal oxides have received great attention due to their special properties such as unique optical properties and special electronic properties as compared to the bulk materials [1, 2]. These properties can be controlled by changing the size of nanoparticles, surface-to-volume ratio, synthesis techniques, and growth temperature [3, 4]. Among the semiconductor nanomaterials, ZnO particles have attracted considerable attention owing to their unique and attractive properties. ZnO particles are *n*-type semiconductors with a wide band gap (3.3–3.6 eV) and a high excitation binding energy of 60 mV at room temperature [5–8]. Moreover, ZnO can be employed in the new generation of semiconductor materials, including photocatalysts, light-emitting diodes, gas sensors [9], solar cells [10], UV-light emitting diodes, and display screens [11–13]. Several physical and chemical methods have been applied in the production of ZnO nanostructures such as solvothermal methods [14], sol-gel, and chemical vapor deposition [15–17]. Furthermore, the combustion synthesis method has been reported as a new, simple, low-cost, and rapid process method, allowing an effective synthesis of ZnO for its industrial production [18]. However, little attention has been focused on the synthesis and study of ZnO nanostructures with metal complexes [19–21]. In the present research, we synthesized complex [Zn(2-Ampy)(Acac)$_2$] (**I**) after that 2-aminopyridine (2-Ampy) and acetyl acetone (Acac) reacted with Zn(CH$_3$COO)$_2$ · 2H$_2$O. We also synthesized complex [Zn(*p*-Van)$_2$(H$_2$O)$_2$] (**II**) after that 4-hydroxy-3-methoxybenzaldehyde (*p*-vanillin) reacted with Zn(ClO$_4$)$_2$ · 6H$_2$O. We prepared ZnO nanoparticles via the solid state thermal decomposition of the Zn(II) complexes. Synthetic procedure for the preparation of complexes **I**, **II** and ZnO nanoparticles are given in Scheme 1:

[1] The article is published in the original.

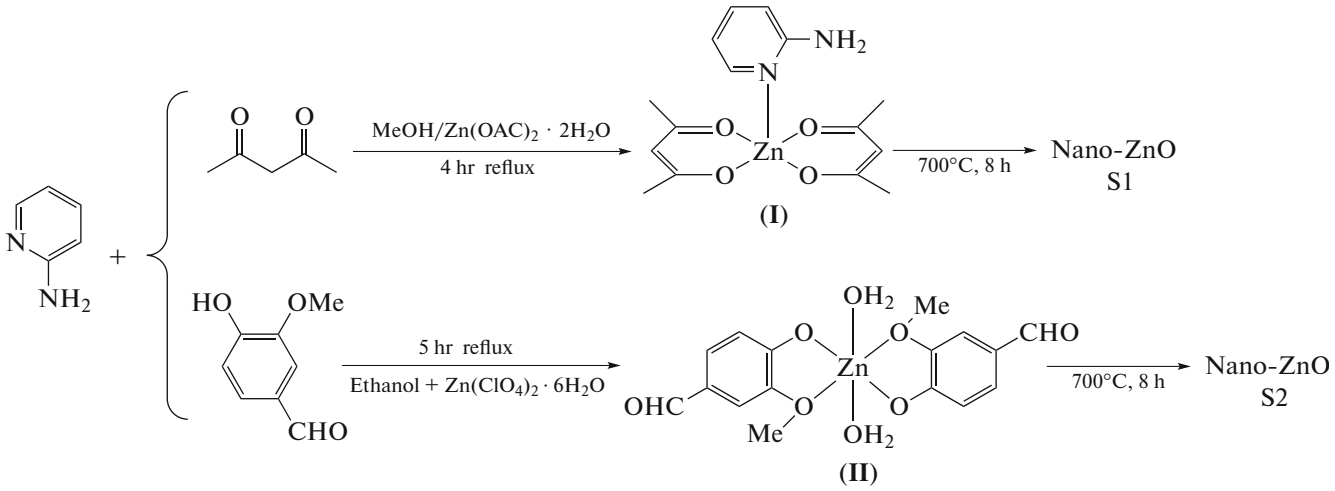

Scheme 1.

EXPERIMENTAL

Materials and physical measurements. All chemicals and solvents were purchased from commercial sources and were used without further purification. FT-IR spectra in KBr plates were obtained on an FT-IR SHIMADZU spectrophotometer. In addition, UV-Vis spectra were recorded on a UV-1650 PC SHIMADZU spectrophotometer in methanol solutions. ^{1}H NMR measurements were performed on an NMR BRUKER 300 MHZ spectrometer, using CD_3OD as the solvent. Powder X-ray diffraction (PXRD) patterns of the complexes were recorded on a Bruker AXS diffractometer D8 ADVANCE with CuK_α radiation. TEM images were obtained from a JEOL JEM 1400 transmission electron microscope (TEM) with an accelerating voltage of 120 kV, and SEM images were collected by a Philips XL-30ESEM (SEM = scanning electron microscopy).

Synthesis of I. Acetylacetone (0.20 g, 2.0 mmol) was dissolved in methanolic (15 mL). To this solution was added 2-aminopyridine (0.19 g, 2.0 mmol) in methanolic (15 mL) and stirred for an hour. Subsequently, a methanol solution of $Zn(CH_3COO)_2 \cdot 2H_2O$ (0.22 g, 1.0 mmol) was added dropwise to the methanolic solution, and the mixture was refluxed for 3 h. Upon slow evaporation of the solvent over 4 days, colorless crystals of complex **I** formed. Cubic colorless crystals of were formed after 1 week.

FT-IR (KBr; ν_{max}, cm^{-1}): 3352 s, 3427 s (N–H). UV-Vis (CH_3OH; λ_{max}, nm (ε, L mol^{-1} cm^{-1})): 233 (31700), 288 (62400). ^{1}H NMR (CD_3OD, 300 MHz): 5.35–7.82 (m., 4H), 6.57 (m., 2H), 1.92(s., 12H).

Synthesis of II. A mixture of 4-hydroxy-3-methoxybenzaldehyde (*p*-vanillin) (0.30 g, 2.0 mmol) and 2-aminopyridine (0.19 g, 2.0 mmol) in ethanol (25 mL) was stirred for an hour at room temperature. Afterwards, an ethanol solution of $Zn(ClO_4)_2 \cdot 6H_2O$ (0.37 g, 1.0 mmol) was added dropwise to the reaction mixture and the resulting solution was refluxed for 4 h. Yellow crystals of complex **II** were formed after five days.

FT-IR (KBr; ν_{max}, cm^{-1}): 1647 s (C=O). UV-Vis (CH_3OH; λ_{max}, nm (ε, L mol^{-1} cm^{-1})): 230 (41800), 280 (31300), 313 (29400). ^{1}H NMR (CD_3OD, 300 MHz): 6.86–7.44 (m., 6H), 9.56 (s., 2H), 3.70 (s., 6H).

Synthesis of ZnO nanoparticles was carried out by the thermal decomposition of the complexes. The complexes were heated at 700°C for 8 h. ZnO nanoparticles, i.e., S1 and S2, were synthesized from complexes **I** and **II**, respectively. The nanoparticles were characterized by FT-IR, XRD, SEM, and TEM.

X-ray crystallography. Diffraction data were collected by ω-scan technique at 130(1) K and room temperature for complexes **I** and **II**, respectively, on Rigaku Super Nova four-circle diffractometer with Atlas CCD detector and mirror-monochromated CuK_α radiation (λ = 1.54178 Å). The data were corrected for Lorentz-polarization and absorption effects [22]. Precise unit-cell parameters were determined by a least-square fit of reflections with the highest intensity (4448 and 2700 for complexes **I** and **II**, respectively) selected from the whole experiment. The structures were solved with SIR92 [23] and were refined with the full-matrix least-square procedure on F^2 by SHELXL-2013 [24]. All non-hydrogen atoms were refined anisotropically. Hydrogen atoms from methyl groups were placed in idealized positions and were refined as "riding model" with isotropic displacement parameters set at 1.5 times U_{eq} of appropriate carrier atoms. All other hydrogen atoms were found in difference Fourier maps and were isotropically refined.

Table 1. Crystallographicdata and structure refinement of complexes **I** and **II**

Parameter	Value	
	I	**II**
Formula	$C_{15}H_{20}N_2O_4Zn$	$C_{16}H_{18}O_8Zn$
Formula weight	357.70	403.67
Crystal system	Monoclinic	Monoclinic
Space group	$P2_1/n$	$C2/c$
a, Å	7.41205(14)	22.1177(9)
b, Å	8.14709(18)	10.5209(4)
c, Å	26.8618(5)	7.7767(3)
β, deg	93.4931(17)	106.871(4)
V, Å^3	1619.08(6)	1731.74(12)
Z	4	4
ρ_{calcd}, g cm^{-3}	1.47	1.55
F(000)	744	832
μ, mm^{-1}	2.28	2.35
θ Range, deg	6.11–73.78	8.05–77.46
Reflections collected/unique	5927/3154	2682/1536
R_{int}	0.045	0.027
Reflections with $I > 2\sigma(I)$	2844	1499
R_1, wR_2 ($I > 2\sigma(I)$)	0.041, 0.101	0.041, 0.108
R_1,wR_2 (all data)	0.045, 0.105	0.041, 0.109
GOOF	1.08	1.08
$\Delta\rho_{max}/\Delta\rho_{min}$, e Å^{-3}	0.88/–0.43	0.61/–0.93

Table 1 lists the relevant crystallography and refinement data.

Crystallographic data for the structural analysis has been deposited with the Cambridge Crystallographic Data Centre (CCDC nos. 1513672 (**I**) and 1513673 (**II**); deposit@ccdc.cam.ac.uk, or www: www.ccdc.cam.ac.uk).

Biological studies. Zinc complexes **I** and **II** were tested against microorganisms, namely *Bacillus subtilis* (*B. subtilis*; PTCC no. 1023; Gram-positive), *Staphylococcus aureus* (*S. aureus*; PTCC no. 1431; Gram-positive), *Enterobacter cloacae* (*E. cloacae*; PTCC no. 1798; Gram-negative), and *Escherichia coli* (*E. coli*; PTCC no. 1399; Gram-negative). The minimal inhibitory concentrations (MIC) of complexes exhibiting no visible growth compared with the drug-free control wells were determined by a broth macrodilution method, using LB broth and final inoculums of 105 and 106 cfu/mL [25, 26]. MBC is the lowest antibiotic concentration required to kill a particular bacterium. To measure the minimum inhibitory concentration (MBC), 100 μL of all clear tubes from a dilution MIC test was spread on Mueller–Hinton agar plates and was incubated at 37°C overnight. Each organism was tested in duplicate on different days to measure the reproducibility of the test. The results obtained were compared with Kanamycin and chloramphenicol as reference standards, and DMSO was also utilized as the positive control.

RESULTS AND DISCUSSIONS

Two new zinc complexes were synthesized and characterized by FT-IR, ^{1}H NMR, UV-Vis (Table 2), and X-ray crystallography. Both complexes were soluble in common organic solvents such as methanol, ethanol, and CH_3CN. Some spectroscopic data for metal complexes in Table 1 are in good agreement with the expected values.

In the FT-IR spectrum of complex **I**, the characteristic peaks at 3352 and 3429 cm^{-1} indicate the existence of NH_2 group in the complex; in addition, the

Table 2. Spectroscopic data for complexes **I** and **II**

Compound	Selected IR[a]	^{1}H NMR (δ, ppm)[b]	UV-Vis (λ_{max}, nm) (ε, L mol^{-1} cm^{-1})[c]
I	3352 s (N–H) 3427 s (N–H)	5.35–7.82 (m., 4H, Ar), 6.57 (m., 2H, CH), 1.92 (s., 12H, CH3)	233 (31700), 288 (62400)
II	1647 s (C=O)	6.86–7.44 (m., 6H, Ar), 9.56 (s., 2H, CH=O), 3.70 (s., 6H, OCH3)	230 (41800), 280 (31300), 313 (29400)

[a] KBr pellets, [b] solvent is CD_3OD, [c] solvent is methanol.

bands around 1658 cm^{-1} are assigned to the C=O vibrations of acetylacetone. The infrared spectrum of the complex **II** shows a peak at 1647 cm^{-1} which is attributed to the stretching vibrations of the aldehyde group (C=O). This peak demonstrates that the aldehyde group does not participate in the formation of bonds with metals. The broad band at 3186 cm^{-1} can be assigned to the stretching vibrations of OH groups in H_2O.

The electronic spectrum of complex **I** in MeOH indicates two peaks at 233 and 288 nm. These peaks can be assigned to intra-ligand $\pi \rightarrow \pi^*$ transitions [27]. For complex **II**, the bands observed at 230, 280, and 313 nm are attributed to the $\pi \rightarrow \pi^*$ transitions of the aromatic ring and C=O group of ligands. The band at 356 nm is attributed to the metal to ligand charge transfer.

^{1}H NMR spectra of the complexes were recorded in CD_3OD. In ^{1}H NMR spectrum of complex **I**, the signal at 1.92 ppm is related to the methyl protons, while that at 5.35 ppm is related to C–H protons. Moreover, the aromatic protons appear in the appropriate region of 6.57–7.82 ppm.

^{1}H NMR spectrum of complex **II** shows a sharp singlet signal at 9.56 ppm, which is assigned to the aldehyde proton (Fig. 1). The aromatic protons appear in the appropriate region of 6.86–7.44 ppm. The singlet signal at 3.70 ppm is attributed to CH_3 protons of methoxy group.

Figure 2 shows the perspective views of complexes **I** and **II**. Table 3 lists some geometrical data. In complex **I**, zinc is five-coordinated by two anionic acetylacetone and 2-aminopyridine ligands in quite regular square pyramidal fashion. However, complex **I** is different. It is C_2 symmetrical (Zn lies on the twofold axis) and six-coordinated (O(6)) by two ligands and two water molecules. The coordination resembles distorted octahedron with one of the angles deviating sig-

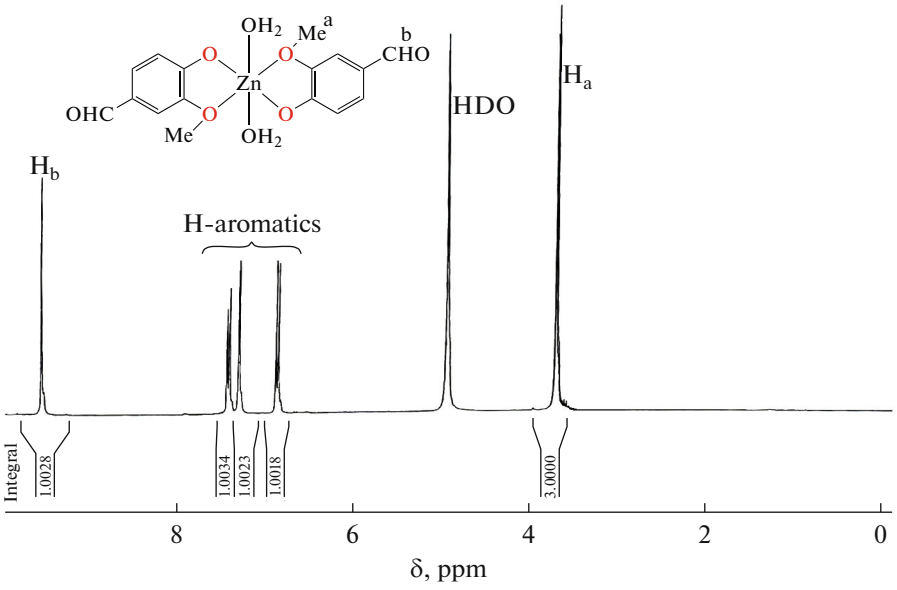

Fig. 1. ^{1}H NMR spectrum of complex **II** in CD_3OD.

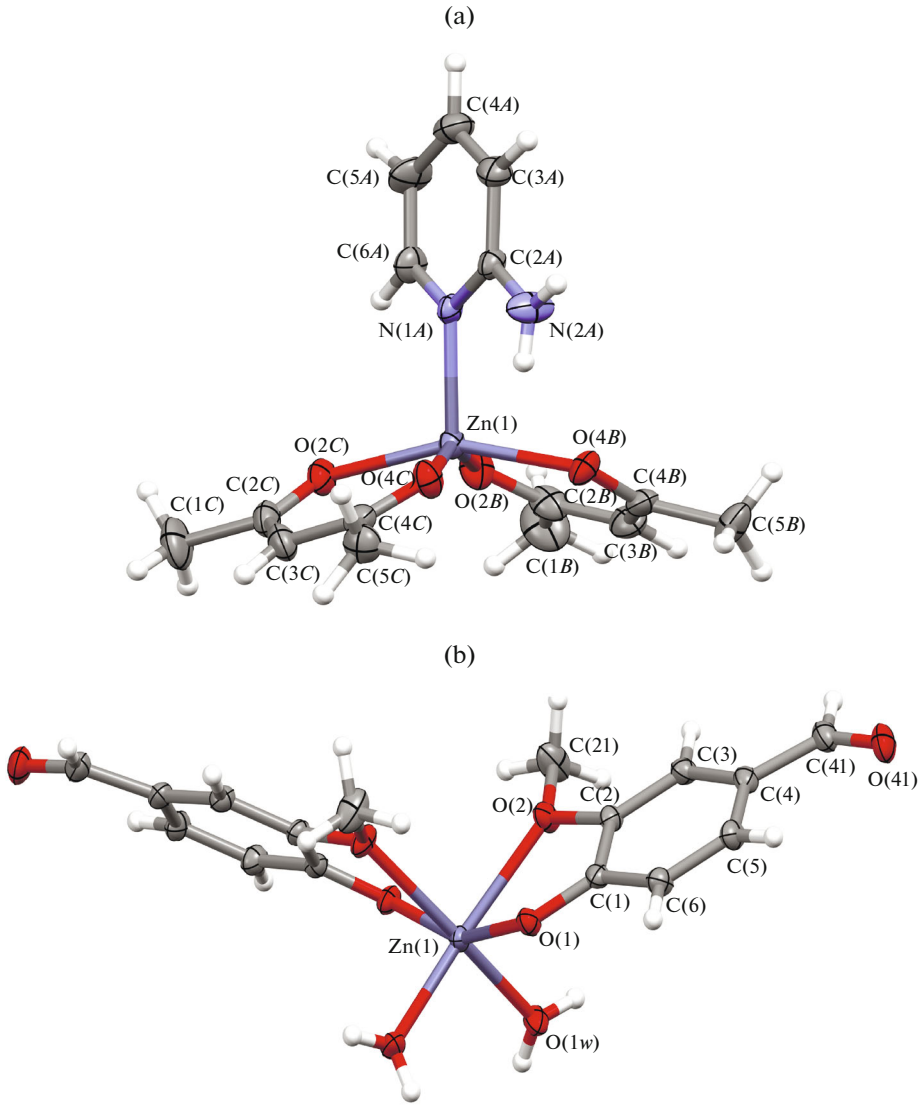

Fig. 2. Perspective view of complexes **I** (a) and **II** (b); ellipsoids are drawn at the 50% probability level; hydrogen atoms are shown as spheres of arbitrary radii.

nificantly from 180°. In the crystal structures of both compounds, hydrogen bonds play an important role. In complex **I**, there are intra- and intermolecular bifurcated N–H···O hydrogen bonds between amino hydrogens and all oxygen atoms, which connect molecules into infinite chains along *x* direction (Fig. 3a). In complex **II**, water molecules connect complexes to centrosymmetric dimers (Fig. 3b) which are further expanded by the other O–H···O hydrogen bonds into a three-dimensional network. Table 4 lists the details of hydrogen bonds.

MIC and MBC of the complexes were tested against four bacteria. Table 5 and Fig. 4 present the biological activities of the metal complexes **I** and **II**. The compounds show a significant antibacterial activity against all test organisms. A comparative study of the MIC and MBC values for the complexes shows activities against *Escherichia coli* and *Enterobacter cloacae*, but complex **I** shows stronger activity against all of the bacteria.

In the FT-IR spectra of zinc oxide (ZnO) nanoparticles obtained from complexes **I** and **II**, the peaks at 400–450 cm^{-1} are attributed to the Zn–O stretching band, which is consistent with that reported before [28]. This band and the absence of the stretching vibrations of organic groups in both complexes indicate the formation of ZnO nanoparticles.

Figure 5 shows the structural analyses performed by FullProf program. The structural analyses were performed by employing profile matching with con-

Table 3. Relevant geometrical data (Å, deg) with s.u.'s in parentheses*

I		**II**	
Bond	*d*, Å	Bond	*d*, Å
Zn(1)–O(2*B*)	2.0134(14)	Zn(1)–O(1)	1.9738(15)
Zn(1)–O(4*B*)	2.0233(12)	Zn(1)–O(1*w*)	2.0383(17)
Zn(1)–O(2*C*)	2.0269(12)	Zn(1)–O(2)	2.3317(15)
Zn(1)–O(4*C*)	2.0308(14)		
Zn(1)–N(1*A*)	2.0674(14)		1.862(2)
Angle	ω, deg	Angle	ω, deg
O(4*B*)Zn(1)O(2*C*)	154.91(5)	O(1*w*)Zn(1)O(2)	171.50(6)
O(2*B*)Zn(1)O(4*C*)	153.90(6)	O(1)Zn(1)O(1)'	155.56(9)

* Prime denoted symmetry code $2 - x, -y, 1 - z$.

stant scale factors. The red lines (*1*) in this figure are the intensities observed, the black ones (*2*) are the data calculated, and the blue ones (*3*) are the difference (Yobs–Ycalc); additionally, the blue bars indicate the positions of Bragg reflections. It was found that the samples were crystallized in a hexagonal crystal structure with the space group of *P*63*mc* [29]. The ratio of peak intensity of the peak at $2\theta = 34.6°$ with the miller indices of (002) to that of the highest peak at $2\theta = 36.2°$ for S2 (517/1107 = 0.46) is smaller than that for S1 (542/648 = 0.83). This smaller ratio is the main difference between PXRD patterns of S1 and S2. Furthermore, the ratio of peak intensity of the peak at $2\theta = 31.7°$ with the miller indices of (100) to that of the highest peak at $2\theta = 36.2°$ for S2 (642/1107 = 0.46) is smaller than that for S1 (724/649 = 1.10). These differences indicate that by changing the reaction condition, the crystal of S2 becomes smaller than that of S1

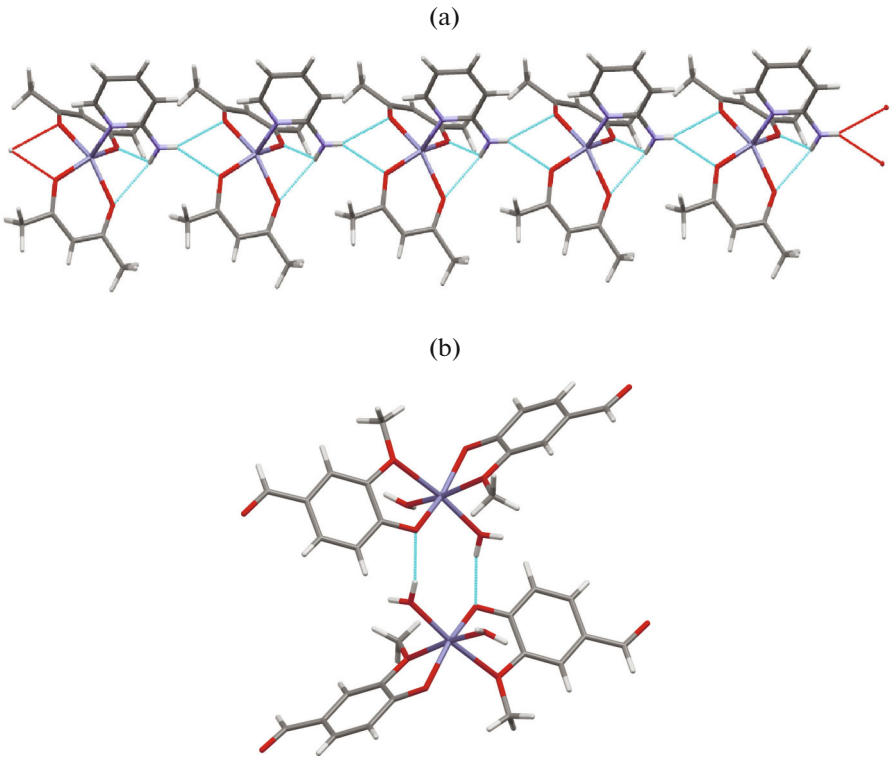

Fig. 3. Hydrogen bonded chain of the complex **I** (a) and hydrogen bonded dimer of complex **II** (b).

Table 4. Geometric parameters of hydrogen bonds of complexes **I** and **II***

D–H···A	Distance, Å			Angle D–H···A, deg
	D–H	H···A	D···A	
I				
N(2*A*)–H(2*A*1)···O(2*B*)[i]	0.75(5)	2.52(4)	3.188(2)	149(4)
N(2*A*)–H(2*A*1)···O(2*C*)[i]	0.75(5)	2.48(5)	3.121(2)	145(4)
N(2*A*)–H(2*A*2)···O(4*B*)	0.83(5)	2.51(5)	3.085(2)	128(3)
N(2*A*)–H(2*A*2)···O(4*C*)	0.83(5)	2.29(4)	3.030(2)	148(4)
II				
O(1*w*)–H(1*w*1)···O(41)[ii]	0.81(4)	1.91(4)	2.717(3)	170(3)
O(1*w*)–H(1*w*2)···O(1)[iii]	0.78(3)	1.94(3)	2.711(2)	168(3)

* Symmetry codes: [i] $1 + x, y, z$; [ii] $-1/2 + x, 1/2 - y, -1/2 + z$; [iii] $2 - x, -y, 2 - z$.

Table 5. MIC and MBC of synthesized compounds against growth of bacteria, μg mL^{-1}

Compound	Gram negative bacteria				Gram positive bacteria			
	E. coli		*E. cloacae*		*S. aureus*		*B. subtilis*	
	MBC	MIC	MBC	MIC	MBC	MIC	MBC	MIC
I	175	150	175	175	250	225	325	250
II	275	250	325	250	500	275	500	500
Kanamycin	4	3.8	3.3	3.2	3.2	3	4	3.6
Chloramphenicol	4.5	4.2	3.5	3.5	2.5	2.4	4.2	4

Table 6. Crystalline parameter data and Rietveld analyses factors of S1 and S2

Sample	Cell parameter		Cell volume, Å	RF	RBragg	X2
	a	*c*				
S1	3.248840	5.204098	54.929053	1.13	1.51	2.4
S2	3.249409	5.204412	54.951611	2.73	3.40	3.14

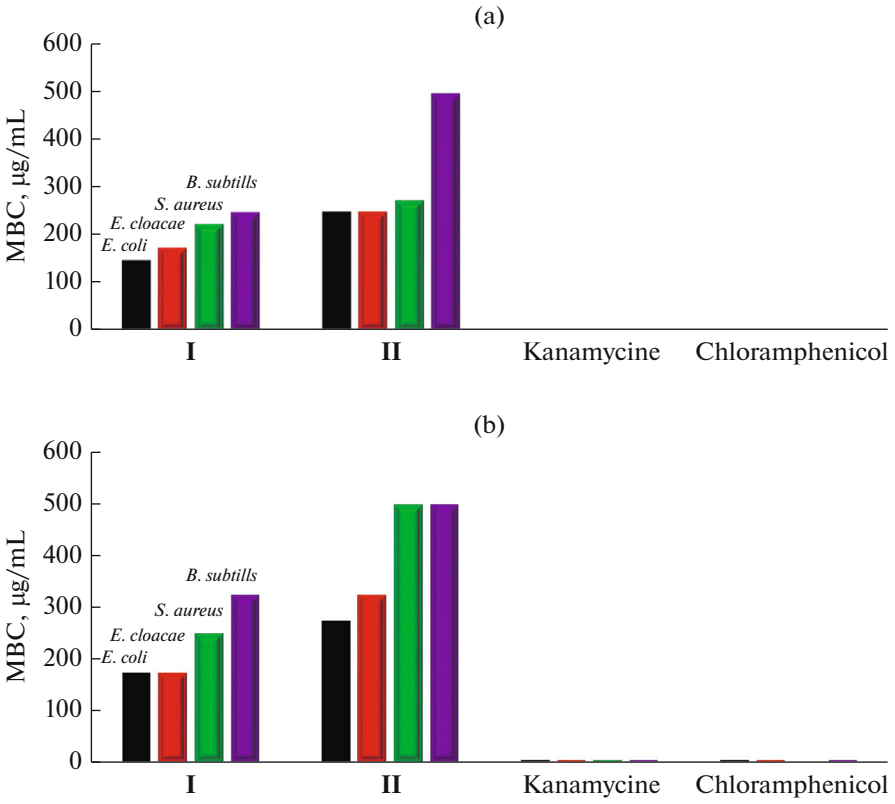

Fig. 4. Histogram showing the comparative activities MIC (a) and MBC (b) of compounds **I** and **II**.

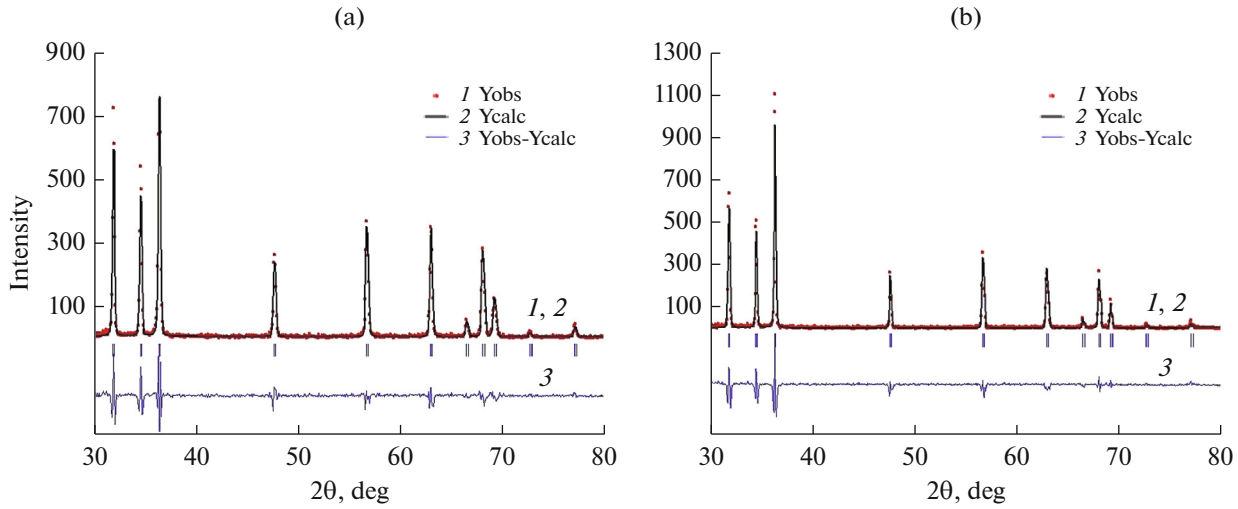

Fig. 5. PXRD patterns and Rietveld analyses of S1 (a) and S2 (b).

at x and z directions. Therefore, according to the above-mentioned data, z direction is the growth direction of the rod in the length size because the direction of S2 is smaller than that of S1. Table 6 shows that the cell parameters are nearly constant, and the cell volume of S2 is a bit larger than that of S1.

Table 7 shows the crystallite sizes of ZnO prepared from complexes **I** and **II** via Scherrer formula (D =

Table 7. Crystalline data for S1 and S2

2θ, deg	θ, deg	β, radian	Cos θ	Crystal size, nm
		S1		
31.77	15.88	0.00336	0.9651	42.63
34.44	17.22	0.00345	0.9551	41.99
36.26	18.13	0.00350	0.9503	41.57
47.50	23.75	0.00392	0.9152	38.56
56.54	28.27	0.00431	0.8807	36.50
62.84	31.42	0.00488	0.8533	33.23
67.91	33.95	0.00502	0.8294	33.24
69.08	34.54	0.00483	0.8237	34.80
		S2		
31.77	15.88	0.00364	0.9651	39.37
34.44	17.22	0.00376	0.9551	38.49
36.26	18.13	0.00394	0.9503	36.97
47.57	23.78	0.00441	0.9150	34.30
56.60	28.30	0.00507	0.8804	30.99
62.910	31.45	0.00535	0.8530	30.32
67.98	33.99	0.00563	0.8291	29.65
69.08	34.54	0.00553	0.8237	30.41

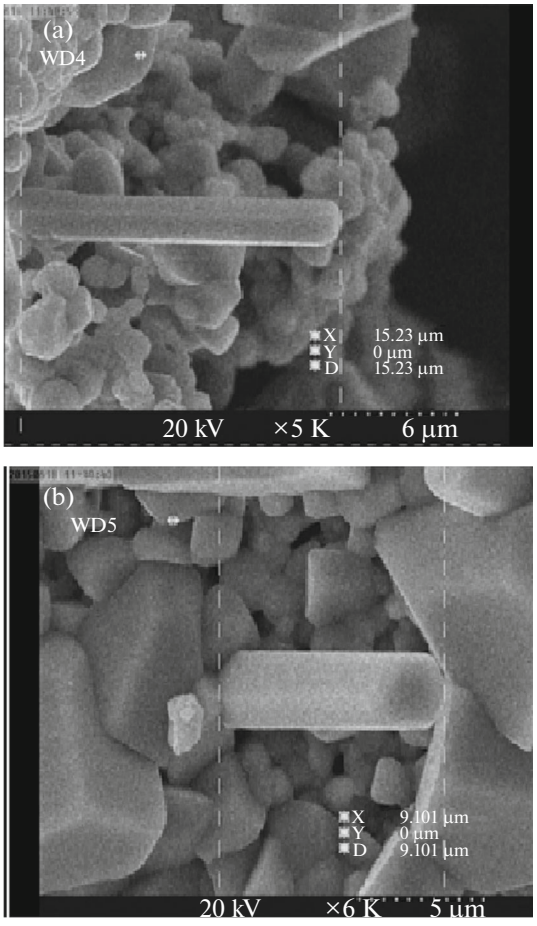

Fig. 6. FESEM images of S1 (a) and S2 (b).

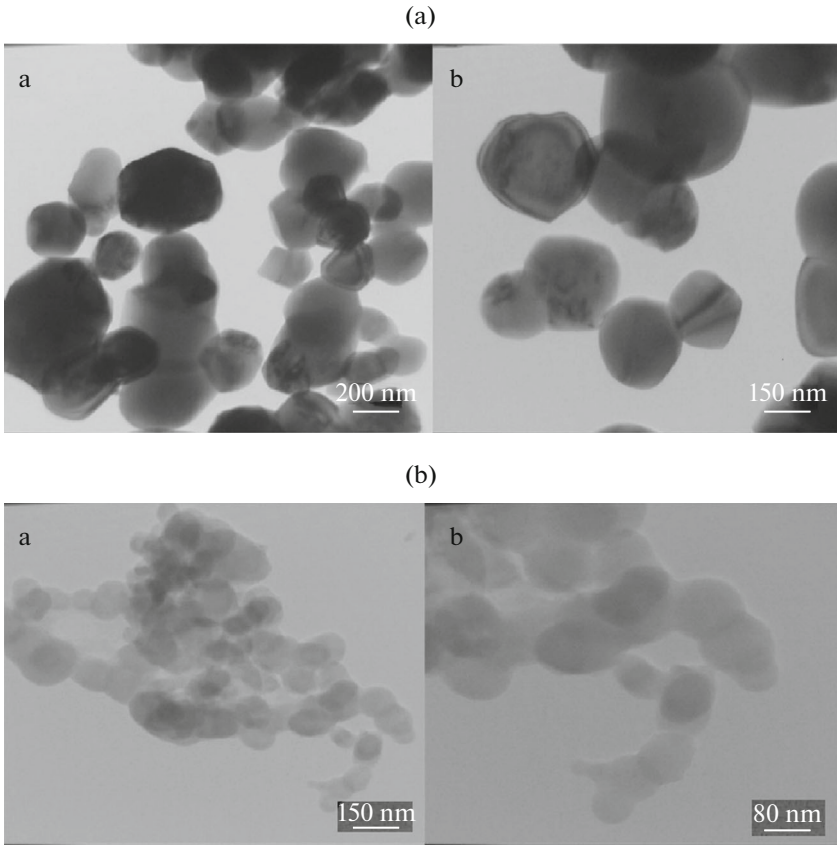

Fig. 7. TEM images of sample ZnO prepared from complexes **I** (a) and **II** (b).

$K\lambda/\beta\cos\theta$) and the peaks. In this formula, D is the average crystalline size, λ is the X-ray diffraction wavelength ($\lambda = 1.5418$ Å), K is the Scherrer constant (0.9), β is the corrected full-width at half-maximum of the diffraction peak, and θ is the Bragg angle [30]. The data demonstrate that the crystallite size of S2 is smaller than that of S1, and the average crystallite size is 37 and 42 nm for S2 for S1, respectively.

In this study, the morphology of ZnO nanoparticles of S1 and S2 is investigated, using scanning electron microscopy (FESEM) and transmission electron microscopy (TEM). Figure 6 presents the FESEM images of S1 and S2. It is obvious that the morphology of the materials obtained is rod and sphere. The sizes of the ZnO nanoparticles obtained via combustion of complexes **I** and **II** and analyzed by TEM are represented in Fig. 7. The morphology both samples S1 and S2 particles is in a nearly spherical shape. According to Figs. 7a, 7b, we found that the particle sizes of S2 are significantly smaller than that of S1. Also, Fig. 8 shows the particle size distribution profiles for S1 and S2 and reveals that the average diameter particle sizes are about 150–200 and 70–80 nm for S1 and S2, respectively. On the basis of FESEM and TEM analysis, it is suggested that parameters, such as reaction temperature, reaction time, and method of synthesis affect the preparation of nanoparticles. Moreover, different precursors play an important role in the formation of the crystalline phase, size, and morphology of ZnO nanoparticles.

Thus in this study, two new Zn(II) complexes were synthesized and characterized by spectral and analytical techniques. The crystal structures of both complexes were determined by X-ray crystallography. Complex **I** had a distorted square pyramid environment, and complex **II** had a distorted octahedral geometry. The ZnO nanoparticles were also prepared by a combustion synthesis method at 700°C for 8 h, using zinc(II) complexes. The structure and morphology of the ZnO nanoparticles synthesized were studied by FT-IR, PXRD, SEM, and TEM. The absence of organic groups in the complexes indicated the formation of ZnO nanoparticles with high purity. The crystallite size estimated by PXRD was approximately 37 and 42 nm for ZnO prepared from complexes **I** and **II**, respectively, showing them to be nano crystalline. It was also found that different precursors have a significant role in the formation of the crystalline phase, morphology, and size of ZnO nanoparticles.

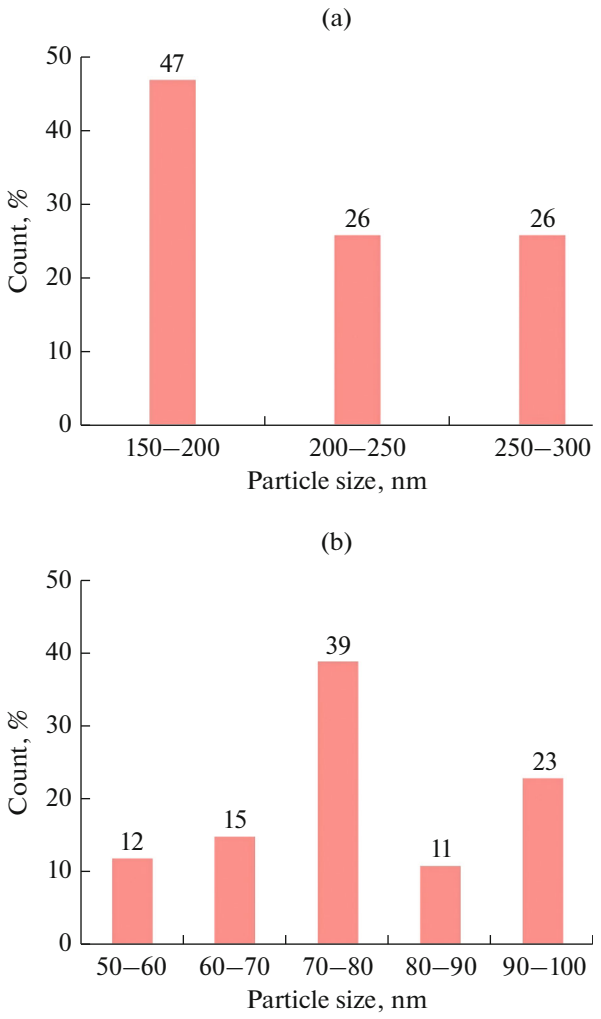

Fig. 8. Particle size distribution profiles of S1 (a) and S2 (b).

ACKNOWLEDGMENTS

Authors gratefully acknowledge the support of the Semnan University.

REFERENCES

1. Askarinezhad, A. and Morsali, A., *Mater. Lett.*, 2008, vol. 62, p. 478.
2. Alammar, T., Birkner, A., Shekhah, O., and Mudring, A.V., *Mat. Chem. Phys.*, 2010, vol. 120, p. 109.
3. Srivastava, R. and Yadav, B.C., *Adv. Mater. Lett.*, 2012, vol. 3, p. 197.
4. Chen, L., Pang, X., and Yu, G., *Adv. Mater. Lett.*, 2010, vol. 1, p. 75.
5. Kim, Y.S., Tai, W.P., and Shu, S.J., *Thin Solid Films*, 2005, vol. 491, p. 153.
6. Li, M., Bala, H., Lv, X., et al., *Mater. Lett.*, 2007, vol. 61, p. 690.
7. Liu, R., Vertegel, A.A., Bohannan, E.W., et al., *Chem. Mater.*, 2001, vol. 13, p. 508.
8. Uthirakumar, P., Karunagaran, B., and Nagarajan, S., *J. Cryst. Growth.*, 2007, vol. 304, p. 150.
9. Sounart, T.L., Liu, J., Voight, J.A., et al., *Adv. Funct. Mater.*, 2006, vol. 16, p. 335.
10. Rau, U. and Schmidt, M., *Thin Solid Films*, 2001, vol. 387, p. 141.
11. Park, N.-K., Lee, Y.J., Han, G.B., et al., *Colloids Surf., A*, 2008, vols. 313–314, p. 66.
12. Service, R.F., *Science*, 1997, vol. 276, p. 895.
13. Sasaki, A., Hara, W., and Matsuda, A., *Appl. Phys. Lett.*, 2005, vol. 86, p. 231911.
14. Hu, Y. and Chen, H.J., *J. Nanopart.*, 2008, vol. 10, p. 401.
15. Wang, Y. and Li, M., *Mater. Lett.*, 2006, vol. 60, p. 266.
16. Wu, C.L., Chang, L., Chen, H.G., et al., *Thin Solid Films.*, 2006, vol. 498, p. 137.
17. Kamalasanan, M.N. and Chandra, S., *Thin Solid Films*, 1996, vol. 288, p. 112.
18. Lee, K.R., Park, S., and Lee, K.W., *Mater. Sci. Lett.*, 2003, vol. 22, p. 65.
19. Salavati-Niasari, M., Davar, F., and Mazaheri, M., *Mater. Lett.*, 2008, vol. 62, p. 1890.
20. Gharagozlo, M. and Naghibi, S., *J. Chin. Chem. Soc.*, 2016, vol. 63, p. 290.
21. Siddiqui, K.A. and Mehrotra, G.K., *J. Coord. Chem.*, 2013, vol. 66, p. 1746.
22. *CrysAlisPro 1.171.38.34a*, Rigaku OD, 2015.
23. Altomare, A., Cascarano, G., Giacovazzo, C., and Gualardi, A., *J. Appl. Cryst.*, 1993, vol. 26, p. 343.
24. Sheldrick, G.M., *Acta Crystallogr., Sect. C: Struct. Chem.*, 2014, vol. 71, p. 3.
25. EUCAST, Determination of Minimum Inhibitory Concentrations of Antibacterial Agents by Agar Dilution, *Clin. Microbiol. Infect.*, 2000, vol. 6, no. 9, p. 509.
26. Ravikumar, S., Gokulakrishnan, R., and Boomi, P., *Asian Pac.J. Trop. Dis.*, 2012, vol. 2, p. 85.
27. Tozzo, E. and Romera, S., dos Santos, M.P., et al., *J. Mol. Struct.*, 2008, vol. 876, p. 110.
28. He, Y., Yang, B., and Cheng, G., *Catal. Today*, 2004, vol. 98, p. 595.
29. *JCPDS, Joint Committee for Powder Diffraction Standards, Power Diffraction File for Inorganic Materials*, 1979.
30. Fallah, H.R., Ghasemi, M., Hassanzadeh, A., and Steki, H., *Physica, B*, 2006, vol. 373, p. 274.